Power Electronics and Drives
Volume 6(41), 2021 DOI: 10.2478/pead-2021-0018

Power Electronics and Drives

The Effect of Different Decision-Making Methods on Multi-Objective Optimisation of Predictive Torque Control Strategy

Research Paper

Aycan Gurel[1], Emrah Zerdali[2,*]

[1] Department of Electrical and Electronics Engineering, Niğde Ömer Halisdemir University, 51200 Niğde, Turkey
[2] Department of Electrical and Electronics Engineering, Ege University, 35100 Izmir, Turkey

Received: October 10, 2021; Accepted: November 08, 2021

Abstract: Today, a clear trend in electrification process has emerged in all areas to cope with carbon emissions. For this purpose, the widespread use of electric cars and wind energy conversion systems has increased the attention and importance of electric machines. To overcome limitations in mature control techniques, model predictive control (MPC) strategies have been proposed. Of these strategies, predictive torque control (PTC) has been well accepted in the control of electric machines. However, it suffers from the selection of weighting factors in the cost function. In this paper, the weighting factor associated with the flux error term is optimised by the non-dominated sorting genetic algorithm (NSGA-II) algorithm through torque and flux errors. The NSGA-II algorithm generates a set of optimal solutions called Pareto front solutions, and a possible solution must be selected from among the Pareto front solutions for use in the PTC strategy. Unlike the current literature, three decision-making methods are applied to the Pareto front solutions and the weighting factors selected by each method are tested under different operating conditions in terms of torque ripples, flux ripples, cur-rent harmonics and average switching frequencies. Finally, a decision-making method is recommended.

Keywords: *predictive torque control • induction motor • multi-objective optimisation • decision-making method*

1. Introduction

Today, a clear trend in the electrification process has emerged in all areas to cope with carbon emissions. For this purpose, the widespread use of electric cars and wind energy conversion systems has increased the attention and importance of electric machines. High-performance control with increased reliability is now the primary goal for these machines, especially induction motors (IMs) and permanent-magnet motors (PMMs). Two mature control techniques, field-oriented control (FOC) and direct torque control (DTC), have been used for a long time. Although both methods have their merits, each method has its limitations as stated in the literature (Wang et al., 2018). Difficulty in designing a cascaded control loop is the main disadvantage of FOC (Wang et al., 2018). On the other hand, DTC has problems with torque ripples, current harmonics and variable switching frequency (Nemec et al., 2007). Therefore, researchers are in search of more advanced control methods.

Model predictive control (MPC) is an emerging topic in the control of power converters and electrical machines. It provides some superiorities over mature control techniques, such as the ability to handle nonlinearities, ease inclusion of additional control objectives, dynamic response and straightforward implementation (Kouro et al., 2009; Rodriguez et al., 2013). Two of the MPC strategies, predictive torque control (PTC) and predictive current control (PCC), are popular in the control of electrical machines. A comparison has been made by (Wang et al., 2015), which concludes that the PTC has lower torque ripples. Also, several comparisons have been made between MPC strategies and mature control techniques in (Rodriguez et al., 2012; Wang et al., 2015). Nevertheless, PTC suffers

* Email: emrah.zerdali@ege.edu.tr

from the weighting factor determination, torque ripples, parameter dependency and variable switching frequency (Rodriguez et al., 2012). Despite the proposed effective solutions, it is still open to research.

The most critical of these disadvantages is the selection of weighting factors as it directly affects control performance. In the traditional approach, these weighting factors are selected by the trial-and-error method which is not an efficient way. Several methods have been proposed to overcome this difficulty and they can be divided into two main groups. The first group of studies (Arshad et al., 2019; Guazzelli et al., 2019; Davari et al., 2021) focuses on the selection methods, while the second group (Rojas et al., 2013, 2017; Zhang and Yang, 2015; Muddineni et al., 2017; Davari et al., 2020; Stando and Kazmierkowski, 2020; Wang et al., 2020; Muddineni et al., 2021) aims to eliminate these factors. Considering the first group of studies, one approach is to optimise these weighting factors with meta-heuristic optimisation algorithms, which has been addressed in a very limited number of papers (Arshad et al., 2019; Guazzelli et al., 2019; Davari et al., 2021). Guazzelli et al. (2019) optimise the weighting factors by a multi-objective genetic algorithm and extensively discuss the results. Although they evaluate three solutions among the Pareto front solutions, a methodology for choosing a final solution is not addressed. To deal with this problem, Arshad et al. (2019) use the Technique for Order of Preference by Similarity to Ideal Solution (TOPSIS) decision-making method for choosing a final solution. In all the mentioned studies, the given problem is considered as a multi-objective optimisation problem and no decision-making method other than TOPSIS has been applied to select a final solution. In addition to these offline selection methods, Davari et al. (2021) use a simplified simulated annealing (SA) algorithm online to tune the weighting factor. In the cost function of SA, a single objective cost function is constructed by scalarising torque and flux error terms, which is called the scalarisation method by Zerdali and Barut (2017). The main disadvantage of this method is the requirement of scalarisation coefficients for both torque and flux error terms. Moreover, it is known that metaheuristic algorithms have an extremely high computational load for real-time implementations. Their micro versions developed for real-time optimisation suffers from low-convergence rates. Gürel and Zerdali (2021) optimise the weighting factor only through speed errors in order to avoid the problems of choosing weighting factors in the scalarisation method and choosing a final solution from the Pareto set in multi-objective optimisation.

In this paper, multi-objective optimisation of the PTC strategy for IM control is performed by the NSGA-II algorithm through flux and speed errors. Unlike the current literature, three decision-making methods are applied to the Pareto front solutions, and the weighting factors selected by each method are tested under different operating conditions in terms of torque ripples, flux ripples, current harmonics and average switching frequencies. Thus, the difficulty in choosing a single solution among the Pareto front solutions can be eliminated.

The rest of this paper is organised as follows. Section 2 introduces the PTC strategy for an IM fed by a two-level voltage source inverter (2L-VSI). Section 3 optimises the PTC strategy with a multi-objective optimisation algorithm and selects one solution by applying different decision-making methods to the Pareto front solutions. Section 4 presents comparison results for the selected weighting factors and gives the statistics for each weighting factor. Finally, Section 5 gives the conclusion.

2. PTC Strategy for IM

Before presenting the PTC strategy, it is always correct to give the mathematical model of IM. For this purpose, first the mathematical model of IM fed with a 2L-VSI is given and then the PTC strategy is presented in detail.

2.1. Mathematic model of IM fed by a 2L-VSI

Mathematical model of the IM can be given the following equation set:

$$\boldsymbol{v}_s = R_s \boldsymbol{i}_s + \frac{d\boldsymbol{\psi}_s}{dt} \tag{1}$$

$$0 = R_r \boldsymbol{i}_r + \frac{d\boldsymbol{\psi}_r}{dt} - j\omega_r \boldsymbol{\psi}_r \tag{2}$$

$$\boldsymbol{\psi}_s = L_s \boldsymbol{i}_s + L_m \boldsymbol{i}_r \tag{3}$$

$$\boldsymbol{\psi}_r = L_m \boldsymbol{i}_s + L_r \boldsymbol{i}_r \tag{4}$$

$$\tau_e = 1.5 p_p \Im m\left(\boldsymbol{\psi}_s^* \cdot \boldsymbol{i}_s\right) \tag{5}$$

$$\frac{d\omega_m}{dt} = \frac{1}{J_t}\left(\tau_e - \tau_l\right) \tag{6}$$

where $\boldsymbol{v}_s = v_{s\alpha} + jv_{s\beta}$ is the voltage vector; $\boldsymbol{i}_s = i_{s\alpha} + ji_{s\beta}$ and $\boldsymbol{i}_r = i_{r\alpha} + ji_{r\beta}$ are the stator and rotor current vectors, respectively; $\boldsymbol{\psi}_s = \psi_{s\alpha} + j\psi_{s\beta}$ and $\boldsymbol{\psi}_r = \psi_{r\alpha} + j\psi_{r\beta}$ are the stator and rotor flux vectors, respectively; R_s and L_s are the stator resistance and inductance, respectively; R_r and L_r are the rotor resistance and inductance, respectively; L_m is the mutual inductance; ω_r and ω_m are the rotor electrical and mechanical angular velocities, respectively; τ_e and τ_l are the electromagnetic torque and load torque, respectively; p_p is the pole-pairs; and J_t is the total inertia.

When the stator terminals of the IM are connected to a 2L-VSI, the stator voltage vectors can be derived as follows:

$$\boldsymbol{v}_s = \frac{2}{3} V_{\text{dc}}\left(S_a + aS_b + a^2 S_c\right) \tag{7}$$

where V_{dc} is the dc-link voltage, $S_x \in \{S_a, S_b, S_c\}$ is the switching state of the upper switches on each leg and *a* is the phase shift of 120 electrical degrees. It is possible to generate seven different voltage vectors with eight possible switching combinations. The circuit topology and voltage vectors can be seen in Figure 1.

2.2. PTC strategy for IM

Block diagram of the PTC strategy for the IM is presented in Figure 2. In this strategy, the optimal voltage vector for next time instant $k+1$ is directly selected through discrete-time IM model and a predefined cost function. First, stator fluxes ($\boldsymbol{\psi}_s^p$) and currents ($\boldsymbol{i}_s^p$) are predicted for each possible voltage vector as in Figure 1b. Using these predicted

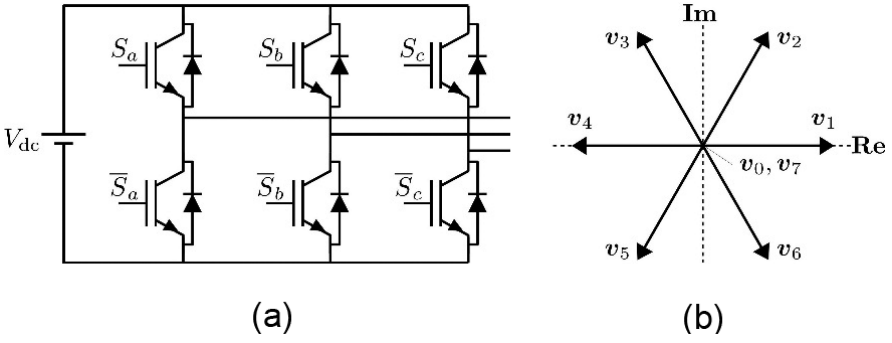

Fig. 1. 2L-VSI (a) Inverter topology (b) Possible voltage vectors. 2L-VSI, two-level voltage source inverter.

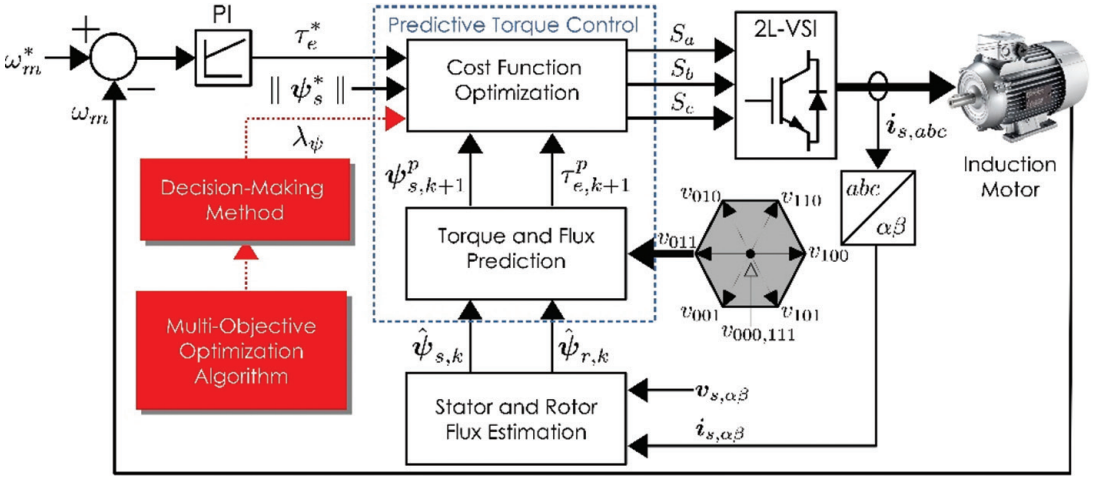

Fig. 2. Block diagram of the PTC strategy for IM control. IM, induction motors; PTC, predictive torque control.

values, the electromagnetic torque (τ_e^p) can be calculated for each possible voltage vector. Finally, one voltage vector with minimum cost value, i.e. optimal voltage vector is selected.

Rotor and stator fluxes are needed in order to predict the values of $\boldsymbol{\psi}_s^p$ and $\boldsymbol{i}_s^p$. Instead of measuring these quantities, $\boldsymbol{\psi}_r^e$ can be estimated using the rotor current model, and $\boldsymbol{\psi}_s^e$ can be derived in terms of $\boldsymbol{\psi}_r^e$.

$$\boldsymbol{\psi}_r^e = \boldsymbol{\psi}_{r,k-1}^e + T\left(R_r k_r \boldsymbol{i}_{s,k} - \left(\frac{1}{T_r} - j\omega_{r,k}\right)\boldsymbol{\psi}_{r,k-1}^e\right) \tag{8}$$

$$\boldsymbol{\psi}_{s,k}^e = k_r \boldsymbol{\psi}_{r,k}^e + L_\sigma \boldsymbol{i}_{s,k} \tag{9}$$

where $k_r = L_m/L_r$, $T_r = L_r/R_r$ and $L_\sigma = L_s - L_m^2/L_r$.

Based on the $\boldsymbol{\psi}_r^e$ and $\boldsymbol{\psi}_s^e$, the $\boldsymbol{\psi}_s^p$ and $\boldsymbol{i}_s^p$ can be predicted as follows:

$$\boldsymbol{\psi}_{s,k+1}^p = \boldsymbol{\psi}_{s,k}^e + T\left(\boldsymbol{v}_{s,k} - R_s \boldsymbol{i}_{s,k}\right) \tag{10}$$

$$\boldsymbol{i}_{s,k+1}^p = \left(1 - \frac{T}{T_\sigma}\right)\boldsymbol{i}_{s,k} + \frac{T}{T_\sigma R_\sigma}\left(k_r\left(\frac{1}{T_r} - j\omega_{r,k}\right)\boldsymbol{\psi}_{r,k}^e + \boldsymbol{v}_{s,k}\right) \tag{11}$$

where $R_\sigma = R_s + k_r^2 R_r$ and $T_\sigma = L_\sigma/R_\sigma$.

Finally, the τ_e^p can be predicted in terms of the $\boldsymbol{\psi}_s^p$ and $\boldsymbol{i}_s^p$ as follows:

$$\tau_{e,k+1}^p = 1.5 p_p \Im m\left(\left(\boldsymbol{\psi}_{s,k+1}^p\right)^* \left(\boldsymbol{i}_{s,k+1}^p\right)\right) \tag{12}$$

In the traditional PTC strategy, the cost function is the sum of the weighted torque and flux errors. The weighting factor for torque errors (λ_τ) is assumed to be one, while the weighting factor for flux errors (λ_ψ) is assumed to be greater than one. Also, an overcurrent protection term I_m can be included as in (13) to prevent the IM from overcurrents.

$$g_j = \lambda_t \left|\tau_e^* - \tau_{e,k+1}^p(j)\right| + \lambda_\psi \left|\left|\boldsymbol{\psi}_s^*\right| - \left|\boldsymbol{\psi}_{s,k+1}^p(j)\right|\right| + I_{m,k+1}(j) \tag{13}$$

The mathematical expression for the overcurrent protection term is as follows:

$$I_{m,k+1}(j) = \begin{cases} 0, & if\left(\left|\boldsymbol{i}_{s,k+1}^p(j)\right| \le \left|\boldsymbol{i}_{s,\max}\right|\right) \\ \infty, & f\left(\left|\boldsymbol{i}_{s,k+1}^p(j)\right| > \left|\boldsymbol{i}_{s,\max}\right|\right) \end{cases} \tag{14}$$

where $|\boldsymbol{i}_{s,\max}|$ is the maximum allowable amplitude of stator current.

3. Multi-Objective Optimisation of the PTC Strategy with Different Decision-Making Methods

In this section, multi-objective optimisation of the PTC strategy is presented in detail and then three different decision-making methods are applied to the Pareto set to choose one of the optimal solutions.

3.1. Multi-objective optimisation of the PTC strategy

This study aims to optimise the weighting factor in the cost function of the PTC strategy over flux and torque errors with an NSGA-II algorithm. The PTC strategy for IM has been implemented in Matlab/Simulink. Also, optimisation toolbox in Matlab has been used for the optimisation of the PTC strategy due to its user-friendly environment. All NSGA-II parameters in Table 1 have been chosen empirically and two cost functions used are as follows:

Table 1. NSGA-II parameters

Parameter	Value	Parameter	Value
Population size	50	Crossover rate	0.8
Max. generation	30	Crossover function	@crossovertwopoint
Lower bound	1	Mutation function	@mutationadaptfeasible
Upper bound	200	Selection function	@tournament
Pareto fraction	1	Tournament size	2

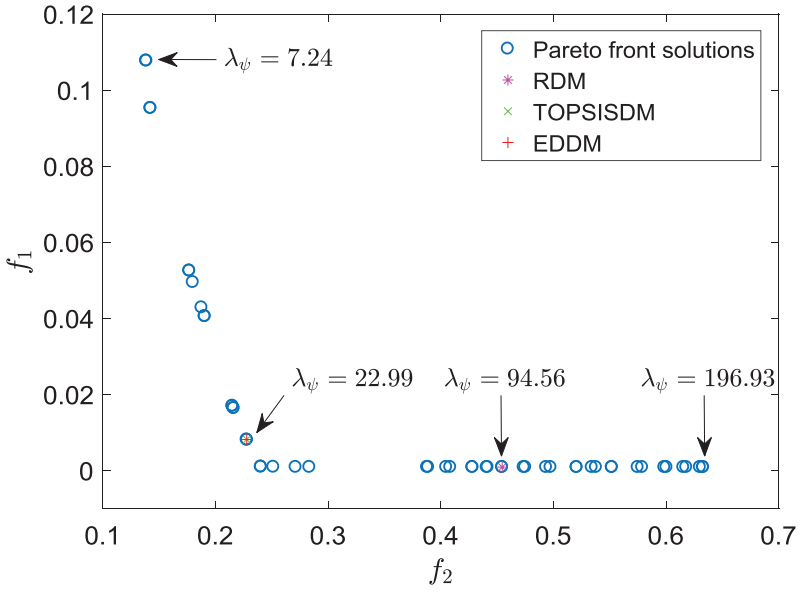

Fig. 3. Pareto front solutions. EDDM, Euclidean distance-based decision-making; RDM, Ranking-based decision-making; TOPSISDM, TOPSIS-based decision-making.

$$f_1 = \frac{1}{n}\sum_{i=1}^{n}\left(\left|\boldsymbol{\psi}_s^*\right| - \left|\boldsymbol{\psi}_s^p\right|\right)^2 \tag{15a}$$

$$f_2 = \frac{1}{n}\sum_{i=1}^{n}\left(\tau_e^* - \tau_e^p\right)^2 \tag{15b}$$

where n is the length of the data captured during the simulation period.

After 30 generations, the NSGA-II algorithm yields an optimal set of solutions, called Pareto front solutions, shown in Figure 3. A reasonable solution should be chosen among them to achieve better control performance. As seen in Figure 3, increasing the λ_ψ value increases the torque errors and decreases the flux errors. Choosing one by the trial-and-error method is a tedious process. So, three new different decision-making methods are applied here to the Pareto front solutions to overcome this challenge.

3.2. Different decision-making methods

This paper studies the effect of different decision-making methods on control performance. For this purpose, three different decision-making methods based on ranking (Rojas et al., 2013), Euclidean distance (Zerdali and Barut, 2017) and TOPSIS (Arshad et al., 2019) are considered.

In the ranking-based decision-making (RDM) method, cost values for each Pareto front solution are independently sorted for each cost function and a ranked value is assigned to a each candidate solution for each cost function. Lower errors correspond to a lower-ranking value. Next, the mean of both ranking values for each candidate solution is calculated and the solution with minimum mean ranking value is chosen. The pseudo-code of the RDM algorithm can be found in Table 2.

Table 2. Pseudo-code of the RDM algorithm

1:	Sort cost values for each cost function independently
2:	Assign a rank value to each cost value for each cost function
3:	Calculate the average ranking score for each point
4:	Select the point with minimum average ranking score

RDM, ranking-based decision-making.

Table 3. Pseudo-code of the Euclidian distance-based decision-making algorithm

1:	Normalise the cost values for each cost function
2:	Calculate the Euclidean distances between the origin and all points
3:	Select the point with minimum Euclidean distance

Table 4. Pseudo-code of the TOPSISDM algorithm

1:	Normalise the cost values for each cost function
2:	Calculate the weighted normalised cost values
3:	Derive the positive and negative ideal solutions for each point
4:	Measure the relative closeness of each point to the positive ideal solution
5:	Select the point with a higher relative closeness coefficient

TOPSISDM, TOPSIS-based decision-making.

In the Euclidean distance-based decision-making (EDDM) method, first the cost values for each fitness function are normalised and then the Euclidean distance between the origin and the point formed by the cost values is calculated for each Pareto front solution. Next, the point with minimum Euclidean distance is selected. The pseudo-code of the EDDM algorithm can be found in Table 3.

In the TOPSIS-based decision-making (TOPSISDM) method, the vectors containing the cost values are created for each cost function and then each vector is separately normalised. A normalised decision matrix is formed by combining these vectors. It is also possible to form a weighted normalised decision matrix by scaling each vector. Then, positive and negative ideal solutions for both vectors are calculated. Finally, the relative closeness of each solution is obtained, and the point with maximum relative closeness value is selected to use. The pseudo-code of the TOPSISDM algorithm can be found in Table 4.

The results obtained after applying the three decision-making methods to Pareto front solutions are marked in Figure 3. Both EDDM and TOPSISDM choose the same weighting factor, i.e. λ_k = 22.99, while the RDM selects λ_k = 94.56 as the weighting factor. Furthermore, the weighting factors for minimum torque error (λ_k = 7.24) and minimum flux error (λ_k = 196.93) are also indicated in Figure 3. It has been experienced during extensive tests that both TOPSISDM and EDDM often choose the same weighting factor or weighting factors which are very close.

4. Results

The PTC strategies with the weighting factors selected by three different decision-making methods are compared taking into account the torque and flux ripples, average switching frequency and total harmonic distortion (THD) of stator currents. A three-phase squirrel cage IM with the rated values and parameters in Table 5 is used. Simulation studies are performed in Matlab/Simulink with a sampling frequency of 20 kHz. The outer speed controller is of PI-type and its proportional and integral gains are 5 and 50, respectively.

To evaluate the performance of decision-making methods, different operating conditions are considered. The details for these scenarios are as follows:

- Low-speed (5 rad/s) test at no-load and under the rated load (20 Nm),
- High-speed (100 rad/s) test at no-load and under the rated load and
- Speed reversal under the rated load.

Table 5. Rated values and parameters of the IM

Parameter	Value	Parameter	Value
P	3 kW	R_s	2.283 Ω
V	380 V	R_r	2.133 Ω
I	6.9 A	L_m	0.22 H
f	50 Hz	L_s	0.2311 H
p_p	2	L_r	0.2311 H
n_m	1,430 r/min	J_t	0.0183 kg/m^2
τ_l	20 Nm	B_t	0.001 N/m/s

IM, induction motors.

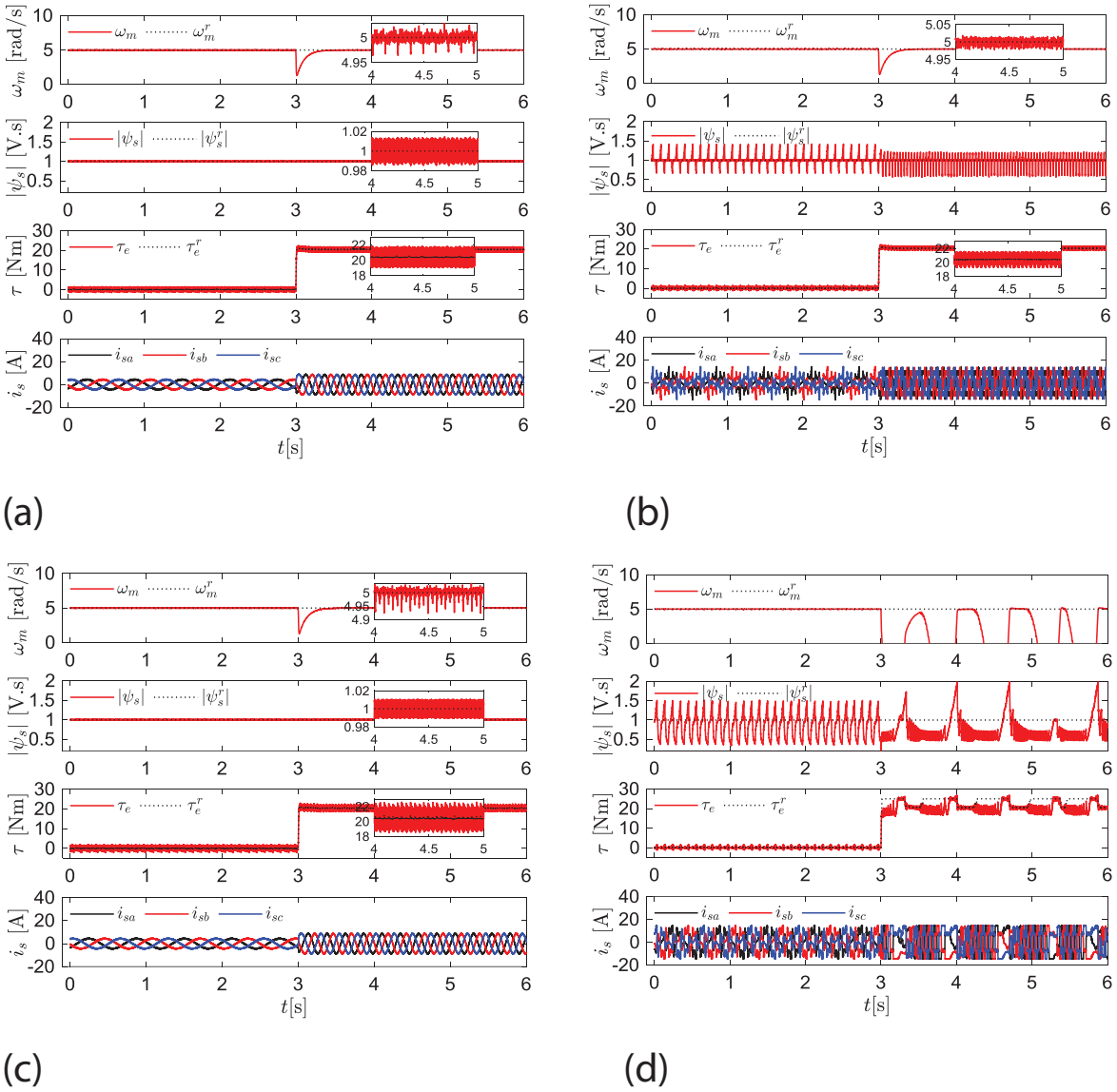

Fig. 4. Control performance at 5 rad/s under load changes. (a) RDM, (b) TOPSISDM and EDDM, (c) λ_k with minimum flux error and (d) λ_k with minimum torque error. EDDM, Euclidean distance-based decision-making; RDM, ranking-based decision-making; TOPSISDM, TOPSIS-based decision-making.

The results for each scenario are presented in Figures 4–6, respectively. In addition to the weighting factors selected by the three different decision-making methods, the results of the weighting factors causing minimum flux and torque errors are also presented in Figures 4–6. Further, root mean square errors (RMSEs) and mean absolute

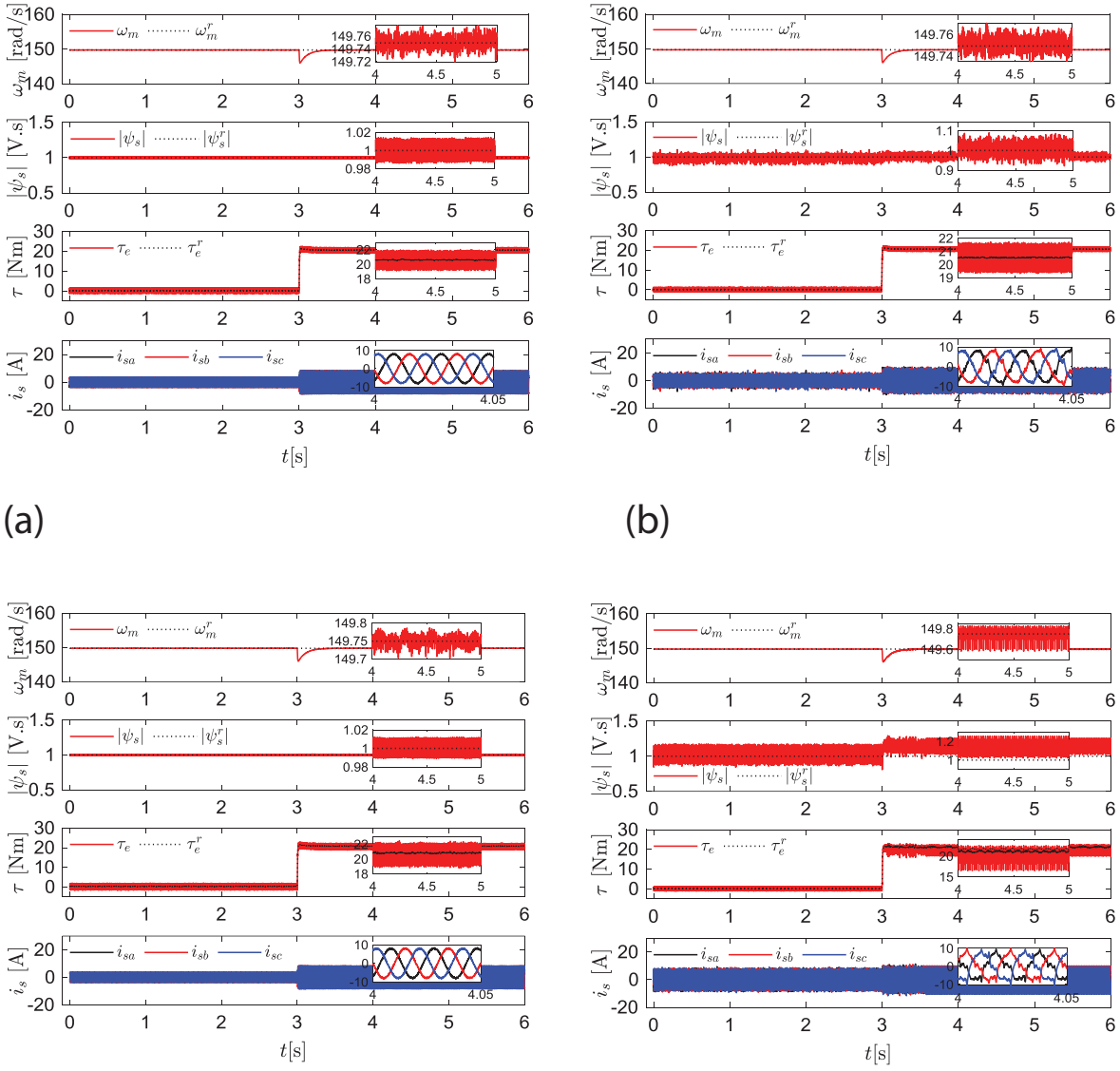

Fig. 5. Control performance at 150 rad/s under load changes. (a) RDM, (b) TOPSISDM and EDDM, (c) λ_x with minimum flux error and (d) λ_x with minimum torque error. EDDM, Euclidean distance-based decision-making; RDM, ranking-based decision-making; TOPSISDM, TOPSIS-based decision-making.

errors (MAEs) for flux, speed and torque errors, to support the results quantitatively, are provided in Table 6. Furthermore, the statistics for each scenario can be seen in Table 7. The statistics given have been calculated using the following mathematical expressions.

$$\chi_{\text{rip}} = \frac{\chi_{\max} - \chi_{\text{avg}}}{\chi_{\text{rated}}} \times 100 \tag{16}$$

where $\chi_{\max}$, χ_{avg}, and χ_{rated} indicate the maximum, average, and rated values of the dummy variable χ, respectively. Flux and torque ripples can be calculated by substituting these quantitates instead of χ.

$$i_{\text{THD}} = 100 \times \sqrt{\left(\frac{I_{\text{rms}}}{I_{1,\text{rms}}}\right)^2 - 1} \tag{17}$$

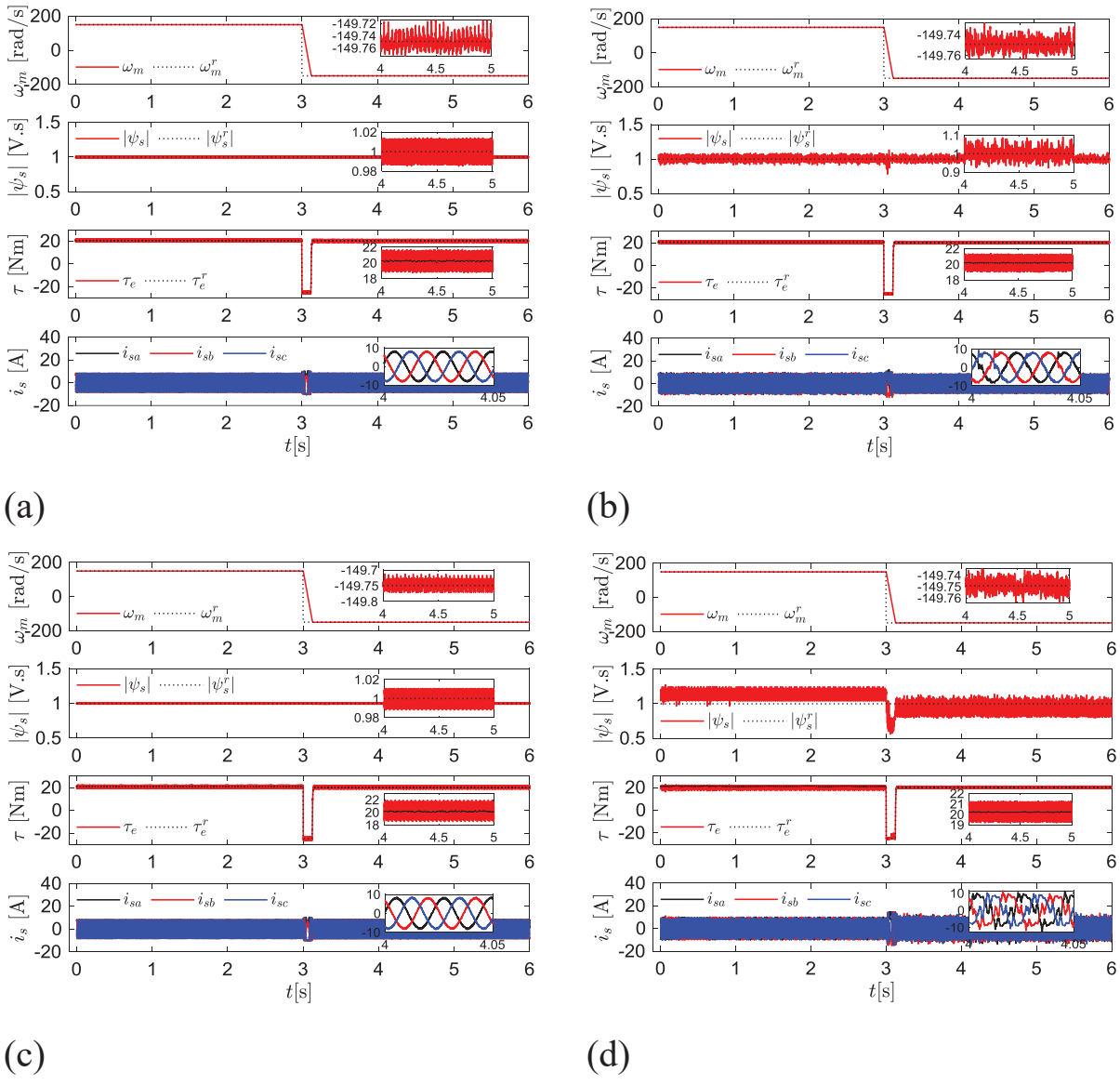

Fig. 6. Control performance under speed reversals at a load of 20 N/m. (a) RDM, (b) TOPSISDM and EDDM (c) λ_k with minimum flux error and (d) λ_k with minimum torque error. EDDM, Euclidean distance-based decision-making; RDM, ranking-based decision-making; TOPSISDM, TOPSIS-based decision-making.

where i_{THD} is the percentage THD of stator current for phase-a. I_{rms} and $I_{1,\mathrm{rms}}$ are root mean square values of phase current and its fundamental component, respectively.

$$f_{\mathrm{avg}} = \frac{N}{n_{sw} \times d} \tag{18}$$

where f_{avg} is the average switching frequency, N is the total state variations in power switches in the time interval of d seconds and n_{sw} is the number of power switches used in the power converter.

The results for the first scenario in Figure 4 demonstrate the importance of weighting factor selection. Improper selection increases THD of stator currents as well as torque and flux ripples. Considering the results in Figure 4 and Tables 6 and 7, It is found that the RDM method has a higher control performance than the TOPSISDM and EDDM methods. Both TOPSISDM and EDDM suffer from large flux ripples and harmonic distortions. When the

Table 6. RMSE and MAE values for speed, flux, and torque errors

		e_{ω}		$e_{\lvert\psi\rvert}$		e_{τ}	
	Method	RMSE	MAE	RMSE	MAE	RMSE	MAE
Figure 4	RDM	0.0011	0.0773	1.6356e−05	0.0047	0.0018	0.5126
	TOPSISDM and EDDM	0.0011	0.0801	3.7735e−04	0.0700	0.0013	0.3665
	λ_k with minimum flux error	0.0011	0.0819	1.3734e−05	0.0039	0.0022	0.6145
	λ_k with minimum torque error	0.0254	4.4070	0.0011	0.3258	0.0091	1.7584
Figure 5	RDM	0.0011	0.0736	1.6763e−05	0.0048	0.0018	0.5248
	TOPSISDM and EDDM	0.0011	0.0710	5.8471e−05	0.0135	0.0013	0.3774
	λ_k with minimum flux error	0.0011	0.0774	1.5247e−05	0.0044	0.0022	0.6195
	λ_k with minimum torque error	0.0011	0.0888	3.0400e−04	0.0937	0.0028	0.5381
Figure 6	RDM	0.0717	3.1021	1.6366e−05	0.0047	0.0019	0.5262
	TOPSISDM and EDDM	0.0717	3.1005	5.3103e−05	0.0121	0.0015	0.3789
	λ_k with minimum flux error	0.0717	3.1044	1.4763e−05	0.0043	0.0022	0.6129
	λ_k with minimum torque error	0.0718	3.1270	3.1176e−04	0.0921	0.0023	0.4763

EDDM, Euclidean distance-based decision-making; MAE, mean absolute errors; RDM, ranking-based decision-making; RMSE, root mean square errors; TOPSISDM, TOPSIS-based decision-making.

Table 7. Statistics for the selected weighting factors

Speed	Load condition	Method	ψ_{rip}(%)	T_{rip}(%)	THD(%)	f_{avg}(kHz)
5 rad/s	Unloaded	RDM	1.4373	7.9100	7.99	0.495
		TOPSISDM and EDDM	41.4168	7.9483	104.53	1.057
		λ_k with minimum flux error	1.1648	9.5245	8.11	0.480
		λ_k with minimum torque error	67.9872	8.0862	239.65	1.425
	20 Nm	RDM	1.5064	7.1744	4.14	1.633
		TOPSISDM and EDDM	24.4676	5.9958	63.00	3.239
		λ_k with minimum flux error	1.0944	11.2602	4.23	1.307
		λ_k with minimum torque error	130.5907	34.8483	372.38	3.359
150 rad/s	Unloaded	RDM	1.5116	7.5986	10.70	8.641
		TOPSISDM and EDDM	10.9377	6.2151	32.54	9.747
		λ_k with minimum flux error	1.1969	9.3206	10.70	8.358
		λ_k with minimum torque error	14.7046	5.8510	100.02	9.987
	20 Nm	RDM	1.4434	7.2562	4.25	9.233
		TOPSISDM and EDDM	8.5045	5.9137	12.70	9.874
		λ_k with minimum flux error	1.2327	9.5934	4.47	9.077
		λ_k with minimum torque error	14.5080	10.1105	23.05	10.074

EDDM, Euclidean distance-based decision-making; RDM, ranking-based decision-making; TOPSISDM, TOPSIS-based decision-making; THD, total harmonic distortion.

remaining weighting factors with minimum flux and torque errors are evaluated, the weighting factor with minimum flux error provides a control performance close to the RDM. Also, it provides a slight reduction in flux fluctuations and switching frequency while slightly increasing torque fluctuations and current harmonics. On the other hand, the weighting factor with minimum torque error loses stability under the rated load.

In the second scenario in Figure 5, although both TOPSISDM and EDDM provide a slight reduction in torque ripples compared to the RDM, this improvement is not sufficient considering flux ripples, current harmonics and switching frequency. Therefore, using the RDM offers a better overall control performance. Similar to the first scenario, using the weighting factor with minimum flux ripples offers a control performance close to the RDM. The weighting factor with minimum torque ripples maintains the stability for this test but it suffers from higher flux and torque ripples, higher current harmonics and higher switching frequencies.

Further, the comments made for the previous two scenarios are also valid for the last scenario shown in Figure 6. The results show that higher values of the weighting factors improve the stability of the PTC strategy, but the optimal decision can be made by using the RDM method that yields a better overall control performance.

The reason for performance degradations at lower values of the weighting factor is that the effect of the flux term in the cost function is reduced and the torque term is more effective in the selection of switching states. This leads to problems with flux stabilisation which hinders correct electromagnetic torque generation. In these cases, more current is requested to generate the reference torque, causing significant current distortions.

5. Conclusion

In this paper, optimisation of the PTC strategy has been performed by a NSGA-II algorithm through the flux and torque errors, and the effect of different decision-making methods on the selection of weighting factors has been compared in terms of flux and torque ripples, current harmonics and switching frequencies. Simulation studies show that the higher values of the weighting factor associated with flux error term improve stability of the PTC strategy, and the RDM method gives the optimal weighting factors. Also, the weighting factor with minimum flux error can be used as an alternative to the RDM. Nevertheless, only one weighting factor has been considered in this paper. Future studies will focus on testing the RDM in the presence of two or more weighting factors.

References

Arshad, M. H., Abido, M. A., Salem, A. and Elsayed, A. H. (2019). Weighting Factors Optimization of Model Predictive Torque Control of Induction Motor Using NSGA-II With TOPSIS Decision Making. *IEEE Access*, 7, pp. 177595–177606. doi: 10.1109/ACCESS.2019.2958415.

Davari, S. A., Norambuena, M., Nekoukar, V., Garcia, C. and Rodriguez, J. (2020). Even-Handed Sequential Predictive Torque and Flux Control. *IEEE Transactions on Industrial Electronics*, 67(9), pp. 7334–7342. doi: 10.1109/TIE.2019.2945274.

Davari, S. A., Nekoukaar, V., Garcia, C. and Rodriguez, J. (2021). Online Weighting Factor Optimization by Simplified Simulated Annealing for Finite Set Predictive Control. *IEEE Transactions on Industrial Informatics*, 17(1), pp. 31–40. doi: 10.1109/TII.2020.2981039.

Guazzelli, P. R., de Andrade Pereira, W. C., de Oliveira, C. M., de Castro, A. G. and de Aguiar, M. L. (2019). Weighting Factors Optimization of Predictive Torque Control of Induction Motor by Multiobjective Genetic Algorithm. *IEEE Transactions on Power Electronics*, 34(7), pp. 6628–6638. doi: 10.1109/TPEL.2018.2834304.

Gürel, A. and Zerdali, E. (2021). Metaheuristic Optimization of Predictive Torque Control for Induction Motor Control. *Ömer Halisdemir Üniversitesi Mühendislik Bilimleri Dergisi*, 11(1). doi: 10.28948/ngumuh.969734.

Kouro, S., Cortes, P., Vargas, R., Ammann, U. and Rodriguez, J. (2009). Model Predictive Control—A Simple and Powerful Method to Control Power Converters. *IEEE Transactions on Industrial Electronics*, 56(6), pp. 1826–1838. doi: 10.1109/TIE.2008.2008349.

Muddineni, V. P., Bonala, A. K. and Sandepudi, S. R. (2021). Grey Relational Analysis-Based Objective Function Optimization for Predictive Torque Control of Induction Machine. *IEEE Transactions on Industry Applications*, 57(1), pp. 835–844. doi: 10.1109/TIA.2020.3037875.

Muddineni, V. P., Sandepudi, S. R. and Bonala, A. K. (2017). Finite Control Set Predictive Torque Control for Induction Motor Drive with Simplified Weighting Factor Selection Using TOPSIS Method. *IET Electric Power Applications*, 11(5), pp. 749–760. doi: 10.1049/iet-epa.2016.0503.

Nemec, M., Nedeljković, D. and Ambrožič, V. (2007). Predictive Torque Control of Induction Machines using Immediate Flux Control. *IEEE Transactions on Industrial Electronics*, 54(4), pp. 2009–2017. doi: 10.1109/TIE.2007.895133.

Rodriguez, J., Kennel, R. M., Espinoza, J. R., Trincado, M., Silva, C. A. and Rojas, C. A. (2012). High-Performance Control Strategies for Electrical Drives: An Experimental Assessment. *IEEE Transactions on Industrial Electronics*, 59(2), pp. 812–820. doi: 10.1109/TIE.2011.2158778.

Rodriguez, J., Kazmierkowski, M. P., Espinoza, J. R., Zanchetta, P., Abu-Rub, H., Young, H. A. and Rojas, C. A. (2013). State of the Art of Finite Control Set Model Predictive Control in Power Electronics. *IEEE Transactions on Industrial Informatics*, 9(2), pp. 1003–1016. doi: 10.1109/TII.2012.2221469.

Rojas, C. A., Rodriguez, J., Villarroel, F., Espinoza, J. R., Silva, C. A. and Trincado, M. (2013). Predictive Torque and Flux Control Without Weighting Factors. *IEEE Transactions on Industrial Electronics*, 60(2), pp. 681–690. doi: 10.1109/TIE.2012.2206344.

Rojas, C. A., Rodriguez, J. R., Kouro, S. and Villarroel, F. (2017). Multiobjective Fuzzy-Decision-Making Predictive Torque Control for an Induction Motor Drive. *IEEE Transactions on Power Electronics*, 32(8), pp. 6245–6260. doi: 10.1109/TPEL.2016.2619378.

Stando, D. and Kazmierkowski, M. P. (2020). Simple Technique of Initial Speed Identification for Speed-Sensorless Predictive Controlled Induction Motor Drive. *Power Electronics and Drives*, 5(1), pp. 189–198. doi: 10.2478/pead-2020-0014.

Wang, F., Li, S., Mei, X., Xie, W., Rodriguez, J. and Kennel, R. M. (2015). Model-based Predictive Direct Control Strategies for Electrical Drives: An Experimental Evaluation of PTC and PCC Methods. *IEEE Transactions on Industrial Informatics*, 11(3), pp. 671–681. doi: 10.1109/TII.2015.2423154.

Wang, F., Zhang, Z., Mei, X., Rodriguez, J. and Kennel, R. (2018). Advanced Control Strategies of Induction Machine: Field Oriented Control, Direct Torque Control and Model Predictive Control. *Energies*, 11(1), pp. 120. doi: 10.3390/en11010120.

Wang, F., Xie, H., Chen, Q., Davari, S. A., Rodriguez, J. and Kennel, R. (2020). Parallel Predictive Torque Control for Induction Machines Without Weighting Factors. *IEEE Transactions on Power Electronics*, 35(2), pp. 1779–1788. doi: 10.1109/TPEL.2019.2922312.

Zerdali, E. and Barut, M. (2017). The Comparisons of Optimized Extended Kalman Filters for Speed-Sensorless Control of Induction Motors. *IEEE Transactions on Industrial Electronics*, 64(6), pp. 4340–4351. doi: 10.1109/TIE.2017.2674579.

Zhang, Y. and Yang, H. (2015). Model-Predictive Flux Control of Induction Motor Drives With Switching Instant Optimization. *IEEE Transactions on Energy Conversion*, 30(3), pp. 1113–1122. doi: 10.1109/TEC.2015.2423692.